A new type of structure of optical fiber pressure sensor based on polarization modulation

Abstract: In this study, a new type of structure of optical fiber pressure sensor (OFPS) based on polarization modulation is proposed, which selects a high-birefringence fiber (HBF) as the sensing unit to measure the pressure in the fluid medium. The PM-1550-01 fiber produced by NTK Photonics Inc. is evaluated as the sample in our subject. Firstly, the regularities of birefringence variation on the PM-1550-01 followed by the external pressure load and the ambient temperature are analyzed by the finite element method (FEM). The results show that the pressure sensitivity is 2.05×10^{-6} RIU/MPa in the pressure range of 0-100 MPa, and the temperature sensitivity is 7.27×10^{-10} RIU/°C in the temperature range of 0-100 °C. Thus, the pressure-temperature cross-sensitivity is only 0.355 kPa/°C in theory. Secondly, the expression of the output light intensity of the introduced OFPS is deduced based on the principles of polarization interference and phase modulation. Combined with simulation results, the measurement ranges of the sensor can be set and adjusted by the length of the sensing unit. Finally, the proposed OFPS is fabricated and external pressure tests within the range of 0-50 MPa are completed. The results show that the pressure sensitivity is approximately 0.145 dB/MPa in the pressure range of 0-44 MPa. There is a fine consistency between the experimental data and simulation results. In addition, the proposed OFPS has many other advantages, such as small size, simple fabrication process and large measurement range, which make it appropriate to be applied in high-pressure measurement in hostile conditions, e.g., downhole and ocean-bottom.

Keywords: optical fiber pressure sensor, high-birefringence fiber, polarization modulation, low temperature cross-sensitivityIntroduction

1. Introduction

In recent years, hydrocarbons resources in the middle and shallow strata are facing the danger of depletion with the growth of world energy demand. Drilling and exploitation of deep and ultra-deep well have become an important development direction of the petroleum industry [1, 2]. With the increase of the well depth, the cost of drilling operation increases rapidly. The accurate collection of bottom hole pressure data, which directly influences the speed and schedule of oil/gas field development, is of great significance for the precise control of oil/gas well drilling and the development of equipment [3, 4]. However, the bottom hole temperature and the pressure of deep wells exceeding 5000 m can generally reach 300 °C and 100 MPa respectively [5, 6]. Under such conditions, the pressure sensors based on electrical principles with inherent limitations present high failure rates. Therefore, due to the obvious advantages such as small size, high sensitivity, long-distance access, corrosion resistance, and electromagnetic interference resistance, the optical fiber pressure sensor (OFPS) has received wide attention from researchers in the field of oil drilling and development [7-13].

At present, fiber Bragg grating (FBG) and Fabry-Perot (F-P) cavities based on pressure sensors have been used for down-hole monitoring [12-15]. However, they still have some limitations in practical applications. Firstly, FBG is easily erased in the high-temperature environment [16, 17]. The new studies have shown that the regenerated FBG technology is expected to solve the problem, but its long-term stability remains a controversial issue [18-20]. Another problem is that the temperature cross-sensitivity existing in the FBG sensor has not been solved yet until now [21, 22]. Secondly, the optical fiber F-P sensors can be classified into the intrinsic F-P interferometric (IFPI) sensors and the extrinsic F-P interferometric (EFPI) sensors [23-25]. IFPI sensors often fabricated by spliced fibers with the properties of simple structure and good robustness, are suitable for mass production and use, but there still exist

several disadvantages including the pressure sensitivity and the temperature cross-sensitivity [26, 27]. By contrast, the EFPI pressure sensors formed between the reflective diaphragm and fiber end-face, have gained wider applications in different branches of industry because of their compact size, high sensitivity, fast response, etc. However, their F-P cavities are quite complicated to fabricate with the requirement of sophisticated equipment and advanced process, which restricts the further development of their application [28, 29].

Generally speaking, each kind of sensor has its own advantage in order to be applied to different requirements, profiting from their sensitivities and measurement ranges which vary with the employed principles, fiber material, and sensitive structures [30-32]. Some long-term studies have demonstrated that various photonic crystal fiber (PCF)-based pressure sensors have higher sensitivity and resolution allowing for a large measurement dynamic range [11, 33, 34]. Likewise, studies also prove that polarization modulation techniques can provide a higher sensitivity compared with other types [11, 35, 36]. Accordingly, the proper design of the PCF pressure sensor combined with polarization modulation technique should be able to improve the pressure sensitivity dramatically. In this study, we propose a new type of structure of OFPS based on polarization modulation, and fabricate its sensing unit using a very short high-birefringence PCF (HB-PCF) to measure pressure in the fluid medium. The embodied performance and low cost enable this type of sensors to have great potential to be promoted.

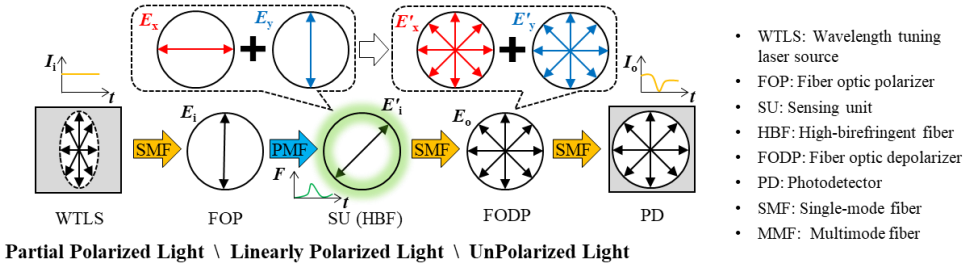

Fig.1. The operating principles of OPFS based on polarization modulation.

2. Working principle

Fused quartz is a type of isotropic optical material, whose refractive index becomes anisotropic under the stress loading condition by the photoelastic effect [37, 38]. In this study, the changes of pressure are measured by the interferometric phase demodulation of the output light with a high-birefringence fiber (HBF) which is used as the sensing unit of the OFPS. The principle of the OFPS is shown in Fig. 1, the beam produced by laser source is converted from the partially polarized light (PPL) to linearly polarized light (LPL) after passing through the polarizer, and incident into the sensing unit at an angle of 45° to the slow axis of the HBF (x-axis). Therefore, the beam at the HBF input end is a set of orthogonal linearly polarized light (OLPL) with the same initial phase and input intensity. Since the two orthogonal polarization modes have different transmission constants β_x and β_y, they will be transmitted independently with the respective polarization state in the x-axis and the y-axis of the HBF. Then, the output beam of the HBF is depolarized to two separate unpolarized lights (UPL) by the depolarizer, the light intensity I_o can be expressed as Eq. (1) on this phase plane.

$$
\begin{aligned}
I_o &= \oint |E_o|^2 = \oint \left|E_x' + E_y'\right|^2 = \left|E_x + E_y\right|^2 \\
&= \left|\frac{1}{2}E_i \cdot e^{-j\phi_x} + \frac{1}{2}E_i \cdot e^{-j\phi_y}\right|^2 \\
&= \frac{1}{4}E_i^2 \cdot \left|e^{-j\phi_x} + e^{-j\phi_y}\right|^2 \\
&= \frac{1}{4}E_i^2 \cdot \left|\cos\phi_x + \cos\phi_y - j\left(\sin\phi_x + \sin\phi_y\right)\right|^2 \\
&= \frac{1}{2}E_i^2 \cdot (1 + \cos k_0 LB)
\end{aligned}
\tag{1}
$$

Where,

$$
\phi_x = \frac{2\pi L \cdot n_x}{\lambda} = k_0 n_x L, \qquad \phi_y = \frac{2\pi L \cdot n_y}{\lambda} = k_0 n_y L
$$

Here, E_i is the electric field intensity of LPL at the sensing unit's input end. E'_i is the electric field intensity of the beam through the HBF, containing two independent components of orthogonal polarization modes. E_o is the electric field intensity of UPL at the sensing unit's output end. Moreover, k_0 is the wave number, L is the length of the HBF, B is the birefringence of the HBF. Φ_x and Φ_y are the differences between the phase of the HBF output and the initial phas, n_x and n_y are effective refractive indexs (ERIs) of the fast-axis mode and slow-axis mode, respectively.

According to Eq. (1), I_o is determined by the input light intensity, namely, the electric field intensity of the LPL. Besides, I_o is also dependent on the three variables of the cosine function, i.e., k_0, L and B. Specifically, k_0 is determined by the wavelength stability of the laser source, L is mainly determined by the temperature, and B is determined by the double effects between the pressure and temperature. Generally, the changes in k_0 and L are very small and can be ignored, moreover, B is more affected by the pressure load than the temperature load from simulation results in Section 3. Through proper variables adjustments, the cosine function $\cos(k_0LB)$ is equal to 1 without the external load, the output light intensity I_o in the depolarizer is maximum, and decreases with the increase of the external pressure load which is affected by the change of birefringence ΔB. Finally, the change of the interference light intensity is observed and analyzed by a photoelectric detector to predict the changes in the external pressure. This is the working principle of the OFPS based on polarization modulation.

3. Design analysis

To prove the effectiveness of pressure measurements based on the designed OFPS structure, an HB-PCF of the PM-1550-01 produced by NTK Photonics Inc. is used as the sensing unit and fully discussed in this section. The pressure-optical and temperature-optical characteristics of the HBF are firstly studied with numerical analysis based on finite element software COMSOL Multiphysics. Then, the length of the sensing unit corresponding to different ranges of the pressure measurement is designed by Eq. (1). Finally, the problems of wavelength stability and temperature cross-sensitivity of the OFPS structure are evaluated and analyzed.

The PM-1550-01 fiber is a kind of the HBF, which is made of pure fused quartz, and a hexagonal air hole structure is distributed around the core area. Since the diameter of two air holes adjacent to the core is bigger than the others, the overall structure of the PM-1550-01 has a clear two-fold symmetry, which makes it show high birefringence. The parameters of the optical fibers used in the numerical simulation are derived from the datasheet of the manufacturer and the references [38], the wavelength of transmission light is 1550 nm. The simulation results show that its EIRs of the fast-axis mode and slow-axis mode are 1.4387 RIU

and 1.4391 RIU, respectively, at a room temperature (20 °C) and zero pressure load (0 MPa). It follows that birefringence B is 4×10^{-4} RIU, and the beat length obtained by counting is 3.94 mm, which is basically consistent with the parameter provided by the manufacturer.

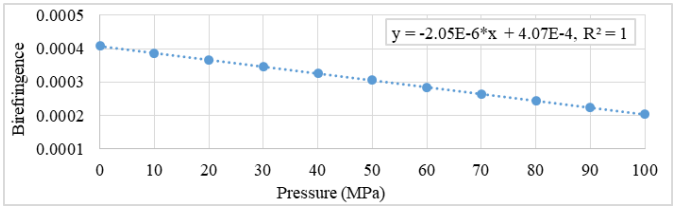

Fig. 2. The pressure-birefringence characteristic of the PM-1550-01, i.e., approximately 10^{-6} RIU/MPa.

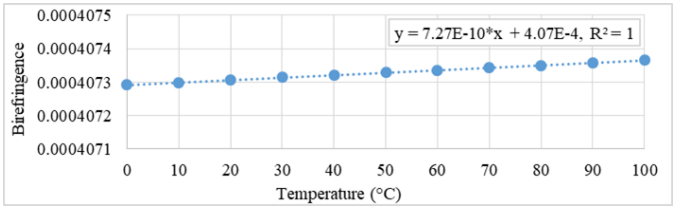

Fig. 3. The temperature-birefringence characteristic of the PM-1550-01, i. e., approximately 10^{-10} RIU/MPa.

Next, the pressure sensitivity and temperature cross-sensitivity of the PM-1550-01 are evaluated in details. The proposed OFPS is set to the specified pressure in the fluid medium, so that the external pressure load on the external surface of the optical fiber is uniformly distributed and directed towards the geometric center. The pressure-birefringence characteristic is numerically analyzed in the pressure range of 0-100 MPa at intervals of 10 MPa in Fig. 2. According to the photoelastic effect, the change of the external pressure load gives a rise to the change of the internal stress distribution. Then it causes the change of ERIs of the fast-axis mode and slow-axis mode. However, due to the difference between the change rates of two ERIs, its birefringence also changes with the pressure, so as to realize the pressure perception. The simulation results are shown in Fig. 2, the birefringence decreases from 4.07×10^{-4} to 2.02×10^{-4} RIU with the external pressure load changing from 0 to 100 MPa. Thus, the pressure sensitivity is 2.05×10^{-6} RIU/MPa, and has a good linear relationship with the birefringence.

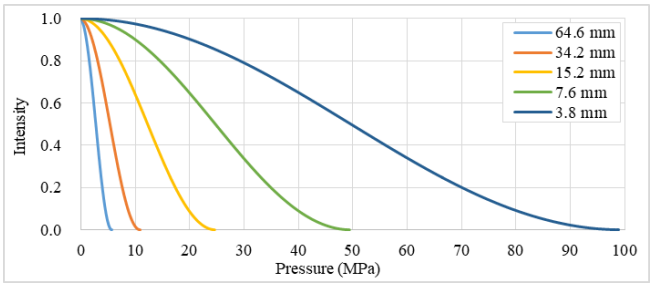

Fig. 4. Relationships between the interference light intensity and the external pressure load from different lengths of the sensing unit by the PM-1550-01.

Generally, the influence of temperature cross-sensitivity is unavoidable to be discussed while the performance of the optical fiber sensor is analyzed. Therefore, the temperature-

birefringence characteristic of the PM-1550-01 is numerically analyzed in the temperature range of 0-100 °C at intervals of 10 °C. The simulation results are shown in Fig. 3, where the temperature sensitivity is only 7.27×10^{-10} RIU/°C. The temperature cross-sensitivity can be calculated as 0.355 kPa/°C in theory. Consequently, the temperature compensation will become a very simple task on account of the fact that the proposed structure of the OFPS will be hardly affected by the distortion of the temperature environment. Especially, there is no need to consider the temperature compensation method in most applications of the high-pressure (MPa Level) measurement.

The external pressure load can be perceived by demodulating the interference light intensity from the proposed OFPS structure based on the pressure-birefringence characteristics of the HBF. However, according to Eq. (1), the change of interference light intensity is expressed as a cosine function, so the range of the pressure measurement needs to be considered in advance, i.e., monotone interval settings of the output light intensity can be achieved by adjusting the length of the sensing unit. The accurate measurement of the pressure within the range can be realized through the mapping relationships between the output light intensity and the external pressure load, which present the characteristics of normalization, continuity, and monotony. The results of the design and analysis are shown in Fig. 4, five maximum target pressures with 5, 10, 20, 40, and 80 MPa can be easily adjusted by changing the length of the PM-1550-01. All changes of the interference light intensity are limited in the monotone interval of the cosine function. It is worth noting that in the design of the pressure sensor, the maximum internal stress value of the inner optical fiber is limited to 1.15 GPa, namely the compressive strength of the fused quartz is at 20 °C [39]. According to the simulation results, the peak of the internal stress reaches 400 MPa when the external pressure load is 100 MPa within the allowable range. Furthermore, the stress concentration induces a bigger difference in the birefringence response, which shows that this kind of the HBF has higher pressure sensitivity.

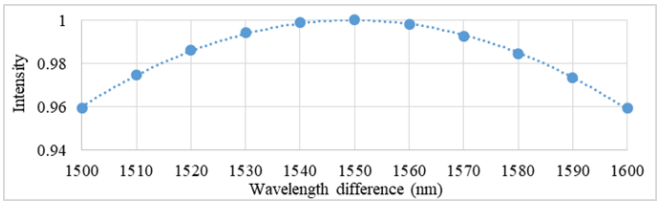

Fig. 5. Relationships between the interference light intensity and the wavelength with a 7.6-mm length PM-1550-01.

The interference light intensity of the OFPS is also affected by the wavelength variation of the laser source according to its operating principle. Here, the sensing unit, namely 7.6-mm-length PM-1550-01, is evaluated in order to make preparations for the practical experiments of the 0-50 MPa pressure measurement. The results are shown in Fig. 5, where the interference light intensity has a peak at 1550 nm. Because the central wavelength stability of the currently used semiconductor laser for optical fiber communication can reach the order of pm, the wavelength shift has a very weak influence on the accuracy of the pressure measurement, which can be ignored. Of course, the property of the stability is especially important. The cosine function in Eq. (1) has three variables of B, L, and k_0. Among them, the former two parameters have differences between the actual value and the estimated value due to the fabrication technique limitations. Especially, they cannot be adjusted after the sensor is fabricated. Fortunately, this problem of the sensor trim can be perfectly solved by adjusting the wavelength of the laser source, namely, changing the wave number k_0.

4. Experiment and evaluation

A proposed OFPS is fabricated and a pressure test is carried out within the 0-50 MPa range. According to the design and principle in section 2, a PM-1550-01 with 7.6-mm length is used as the sensing unit, where a polarization-maintaining fiber (Fujikura Ltd., SM15-PS-U25D) and a single-mode fiber (Corning Inc., SMF-28e) are fused to both ends as the input fiber and output fiber, respectively. In this study, an automated fiber fusion splicer (Sumitomo Electric Industries Ltd., Type-81C) is used, where the manual mode is taken for welding. The fiber position, end face spacing, discharge time and strength are optimized in the earlier stage of the experiments.

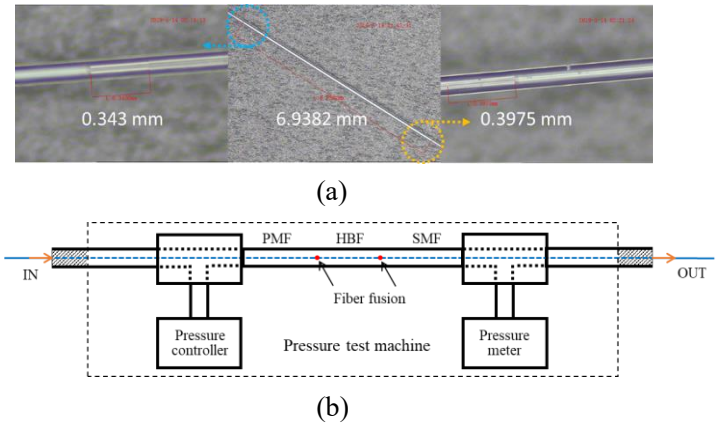

Fig. 6. Sensor production and evaluation. (a) Image of the fabricated sensing unit with a 6.94 mm-length PM-1550-01, the dotted circle portions show air holes collapsing about 0.3 to 0.4 mm length. (b) An image of the pressure measurement system structure.

The fabricated sensing unit is shown in Fig. 6(a), the unchanging portion of the PM-1550-01 is about 6.94 mm, and the ends of the fiber have the air holes collapsing with 0.3 to 0.4 mm due to arc-fusion splicing. Certainly, these values have some errors because they are observed through the optical microscope, and it cannot be effectively evaluated whether the visible collapsing portion of the fiber completely loses the polarization maintaining characteristic or not. This problem needs to be estimated based on the interferometric phase demodulation of the output light. The pressure environment where the medium is pure water, is set up by using the pressure test machine in the range of 0-60 MPa. As shown in Fig. 6(b), the sensing unit and portions of the input and output fibers are placed in a through-type pipe and encapsulated at both ends with epoxy. The pressure is evaluated by using a relative pressure gauge with the range from -100 kPa to 60 MPa, which has an accuracy of 0.05% fs.

The experiment on the system structure is as shown in Fig. 1, a tunable laser (Keysight 81606A-116) and a power sensor (Keysight 81636B) are used to evaluate the relationships between the interference light intensity and the external pressure load. An optical fiber polarizer (Thorlabs ILP1550SM-FC) and an optical fiber depolarizer (Bonphot Optoelectronics DPOL-S-B-1-2) are used to produce polarization and remove polarization. In order to reduce the influence of heat release caused by the medium being quickly compressed, the temperature change of the pressure chamber is monitored in all experimental procedures, the pressure test of the OFPS is implemented at 25±1 °C.

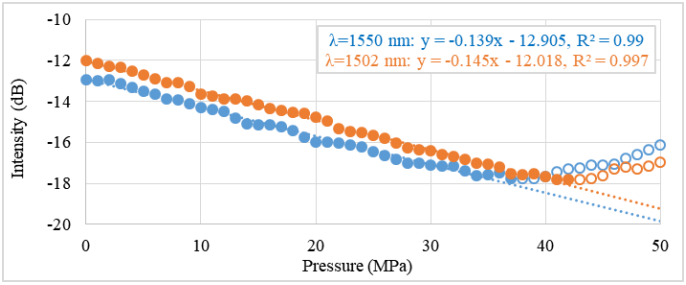

Fig. 7. Relationships between the interference light intensity and the external pressure load.

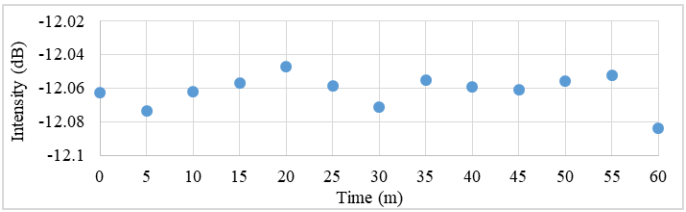

Fig. 8. The stability of the output light intensity at a room temperature and zero pressure load.

Firstly, the relationship between the interference light intensity and the external pressure load is analyzed at 1550 nm. As shown in the blue scatter plots of the Fig. 7, a minimum value appears at 37 MPa, the pressure sensitivity has -0.139 dB/MPa in the left monotonic interval, and the decisive coefficient R^2 is 0.99. The root mean squared error (RMSE) between the linear regression and the measured power shift is 0.152 dB, and a maximum error is 0.427 dB. Secondly, the pressure test machine is adjusted to 0 MPa external pressure load. It follows that the output light intensity has a maximum value at 1502 nm by tuning of laser wavelength. Likewise, the relationship between the interference light intensity and the external pressure load is analyzed at 1502 nm. The orange scatter plots of the Fig. 7 show a minimum value at 44 MPa, its pressure sensitivity is -0.145 dB/MPa in the left monotonic interval, and the decisive coefficient R^2 is 0.997. The RMSE between the linear regression and the measured power shift is 0.101 dB, and a maximum error is about 0.154 dB. Finally, the stability of the fabricated OFPS is evaluated. The changes in the output light intensity are smaller than 0.04 dB in 1 hour at a room temperature and zero pressure load. The RMSE is 0.01 dB.

These errors mainly come from two aspects. One is from pressure instability by the test machine with an accuracy of 0.05% fs. The other one is from the interference of the laser source, including power instability, electronic noise and environmental factor. The former does not affect the detecting accuracy of the OFPS, while the latter can be reduced or eliminated by adding a reference optical path and using a balanced photodetector to suppress noise in subsequent studies. Despite such solutions, the stabilities of the electronic units such as lasers and detectors are still very important in the application of this type of optical sensor. In addition, these experimental data from 6.94-mm-length sensing unit is very similar to the simulation results from the 7.6-mm-length sensing unit. There are two possibilities that can explain this phenomenon. One is that the air holes collapsing portions of the PM-1550-01 do not completely lose polarization-maintaining characteristic. The other is that the simulation results of the pressure-birefringence characteristics have some minor errors, the actual value should be larger. The true reason still needs further verification in future work.

Table 1
Comparison of main sensor parameters reported by research groups.

Work	Pressure sensitivity	Pressure ranges (MPa)	Temperature cross-sensitivity (kPa/K)
Our	0.145 dB/MPa	0-44	0.355
Ref. 5	-294.69 nm/MPa	0-100	6
Ref. 6	12 pm/MPa	0-100	958
Ref. 12	-141.42 nm/MPa	2-72	Not reported
Ref. 15	1.071 rad/MPa	2-120	2.488
Ref. 40	0.33 pm/MPa	0-140	0.6

For a clearer comparison, Table 1 shows pressure sensitivity, pressure range and temperature cross-sensitivity of the proposed OFPS and the main high-pressure sensors (greater than 30 MPa) in the literature. It is obvious that each of the methods has its own advantages and limitations as described in Section 1. Our work has a comparative advantage in temperature cross-sensitivity. In addition, the result of the literature [40] also shows a low cross-sensitivity based on an FBG sensor written in specialty fiber. This also offers an attractive solution that sensors using optical fiber are more sensitive to pressure, for example, endlessly single-mode photonic crystal fiber with high birefringence for sensing applications [41].

5. Conclusions

In this study, a new type of structure of OFPS based on polarization has been proposed and demonstrated for measuring the pressure in a fluid medium. The research results indicate that the fabricated OFPS by the PM-1550-01 fiber shows a pressure sensitivity of 0.145 dB/MPa in the external pressure test from 0 to 44 MPa. Combined with the theoretical temperature cross-sensitivity of 0.355 kPa/°C, it has significant advantages in high-pressure measurement applications with large temperature variations. In addition, this type of the OFPS is fabricated by easy and affordable methods, which only include fiber cleaving and fusion. Furthermore, the simple and strong structure makes this type of sensor suitable for pressure measurement under harsh conditions, such as downhole and seabed. The deficiency of this work is limited to a maximum pressure of 50 MPa by experimental conditions, far from the theoretical limit of the PM-1550-01 fiber. In the next phase, a 120 MPa high-voltage test bench is planned to be taken to test the pressure sensitivity and other properties of the fabricated OFPS in an extremely high-pressure environment. Moreover, the packaging effect on the sensor's performance is also an important concern needed to be focused on.

Funding

This work was supported by the Fundamental Research Funds for the Central Universities (Grant No. 22120180189 and No. 22120190009) and National Natural Science Foundation of China (Grant No. 61873189).

References

[1] Fridleifsson G, Elders WA, Zierenberg RA, Stefánsson A, Fowler APG, Weisenberger TB, et al. The Iceland Deep Drilling Project 4.5 km deep well, IDDP-2, in the seawater-recharged Reykjanes geothermal field in SW Iceland has successfully reached its supercritical target. Sci Drill 2017;23:1. https://doi.org/10.5194/sd-23-1-2017.

[2] Liao X, Wang CY. Seasonal Permeability Change of the Shallow Crust Inferred From Deep Well Monitoring. Geophys Res Lett 2018;45:11,130. https://doi.org/10.1029/2018GL080161.

[3] Karimi Vajargah A, van Oort E. Early kick detection and well control decision-making for managed pressure drilling automation. J Nat Gas Sci Eng 2015;27:354. https://doi.org/10.1016/j.jngse.2015.08.067.

[4] Vaferi B, Eslamloueyan R, Ghaffarian N. Hydrocarbon reservoir model detection from pressure transient data using coupled artificial neural network—Wavelet transform approach. Appl Soft Comput J 2016;47:63. https://doi.org/10.1016/j.asoc.2016.05.052.

[5] Li H, Zhao QZ, Jiang SD, Ni JS, Wang C. FP cavity and FBG cascaded optical fiber temperature and pressure sensor. Chinese Opt Lett 2019;17:040603. https://doi.org/10.3788/col201917.040603.

[6] Qiao X, Shao Z, Bao W, Rong Q. Fiber bragg grating sensors for the oil industry. Sensors 2017;17:429. https://doi.org/10.3390/s17030429.

[7] Leal-Junior A, Marques C, Frizera A, Pontes MJ. Multi-Interface Level in Oil Tanks and Applications of Optical Fiber Sensors. Opt Fiber Technol 2018;40:82. https://doi.org/10.1016/j.yofte.2017.11.006.

[8] Leal-Junior A, Díaz C, Frizera A, Marques C. Simultaneous measurement of pressure and temperature with a single FBG embedded on a polymer diaphragm. Opt Laser Technol 2019;112:77. https://doi.org/10.1016/j.optlastec.2018.11.013.

[9] Leal-Junior A, Frizera A, Díaz C, Marques C, Ribeiro M, Pontes MJ. Material features based compensation technique for the temperature effects in a polymer diaphragm-based FBG pressure sensor. Opt Express 2018;26:20590. https://doi.org/10.1364/OE.26.020590.

[10] Baldwin C. Fiber Optic Sensors in the Oil and Gas Industry: Current and Future Applications. Elsevier Inc.; 2018. https://doi.org/10.1016/B978-0-12-803131-5.00008-8.

[11] Hameed MFO, Obayya S. Computational photonic sensors. Springer International Publishing; 2018. https://doi.org/10.1007/978-3-319-76556-3.

[12] Zhou X, Yu Q, Peng W. Fiber-optic Fabry–Perot pressure sensor for down-hole application. Opt Lasers Eng 2019;121:289. https://doi.org/10.1016/j.optlaseng.2019.04.028.

[13] Huang JY, Van Roosbroeck J, Vlekken J, Kinet D, Martinez AB, Geernaert T, et al. Effect of hydrogen gas on FBG-based optical fiber sensors for downhole pressure and temperature monitoring. Opt Express 2019;27:5487. https://doi.org/10.1364/oe.27.005487.

[14] Yamate T, Fujisawa G, Ikegami T. Optical Sensors for the Exploration of Oil and Gas. J Light Technol 2017;35:3538. https://doi.org/10.1109/JLT.2016.2614544.

[15] Qi XG, Wang S, Jiang JF, Liu K, Wang X, Yang YG, Liu TG. Fiber Optic Fabry-Perot Pressure Sensor with Embedded MEMS Micro-Cavity for Ultra-High Pressure Detection. J Light Technol 2019;37:2719. https://doi.org/10.1109/JLT.2018.2876717.

[16] Wu W, Liu X. Investigation on high temperature characteristics of FBG sensors. Optik (Stuttg) 2015;126:2411. https://doi.org/10.1016/j.ijleo.2015.06.009.

[17] Rinaudo P, Paya-Zaforteza I, Calderón P, Sales S. Experimental and analytical evaluation of the response time of high temperature fiber optic sensors. Sensors Actuators, A Phys 2016;243:167. https://doi.org/10.1016/j.sna.2016.03.022.

[18] Chah K, Yüksel K, Kinet D, Yazd NS, Mégret P, Caucheteur C. Fiber Bragg grating regeneration at 450°C for improved high temperature sensing. Opt Lett 2019;44:4036. https://doi.org/10.1364/ol.44.004036.

[19] Yang HZ, Paul MC, Das S, Dhar A, Qiao XG, Nazal NAM, Lim KS, Ahmad H. Regenerated grating produced in a multimaterial glass-based photosensitive fiber with an ultrahigh thermal regeneration ratio. Opt Express 2019;27:4329. https://doi.org/10.1364/oe.27.004329.

[20] Wang RZ, Si JH, Chen T, Yan L, Cao HJ, Pham X, Hou X. Fabrication of high-temperature tilted fiber Bragg gratings using a femtosecond laser. Opt Express 2017;25:23684. https://doi.org/10.1364/oe.25.023684.

[21] Liu W, Guo Y, Xiong L, Kuang Y. Fiber Bragg grating based displacement sensors: state of the art and trends. Sens Rev 2019;39:87. https://doi.org/10.1108/SR-06-2017-0116.

[22] Wu H, Guo Y, Xiong L, Liu W, Li G, Zhou X. Optical Fiber-Based Sensing, Measuring, and Implementation Methods for Slope Deformation Monitoring: A Review. IEEE Sens J 2019;19:2786. https://doi.org/10.1109/JSEN.2019.2891734.

[23] Rajibul Islam M, Mahmood Ali M, Lai MH, Lim KS, Ahmad H. Chronology of fabry-perot interferometer fiber-optic sensors and their applications: A review. Sensors (Switzerland) 2014;14:7451. https://doi.org/10.3390/s140407451.

[24] Domingues MF, Rodriguez CA, Martins J, Tavares C, Marques C, Alberto N, Andre P, Antunes P. Cost-effective optical fiber pressure sensor based on intrinsic Fabry-Perot interferometric micro-cavities. Opt Fiber Technol 2018;42:56. https://doi.org/10.1016/j.yofte.2018.02.016.

[25] Fu X, Lu P, Zhang J, Qu Z, Zhang W, Li Y, Hu P, Yan W, Ni WJ, Liu DM, Zhang JS. Micromachined extrinsic Fabry-Pérot cavity for low-frequency acoustic wave sensing. Opt Express 2019;27:24300. https://doi.org/10.1364/oe.27.024300.

[26] Wu J, Yao M, Xiong F, Ping Zhang A, Tam HY, Wai PKA. Optical Fiber-Tip Fabry-Pérot Interferometric Pressure Sensor Based on an in Situ μ-Printed Air Cavity. J Light Technol 2018;36:3618.

https://doi.org/10.1109/JLT.2018.2843885.

[27] Ghildiyal S, Ranjan P, Mishra S, Balasubramaniam R, John J. Fabry-Perot Interferometer-Based Absolute Pressure Sensor With Stainless Steel Diaphragm. IEEE Sens J 2019;19:6093. https://doi.org/10.1109/JSEN.2019.2909097.

[28] Wen N, Ping L, Xin F, Wei Z. Ultrathin graphene diaphragm-based extrinsic Fabry-Perot interferometer for ultra-wideband fiber optic acoustic sensing. Opt Express 2018;26:20758. https://doi.org/10.1364/oe.26.020758.

[29] Poeggel S, Duraibabu D, Tosi D, Leen G, Lewis E. Femtosecond-Laser-Based Inscription Technique for Post-Fiber-Bragg Grating Inscription in an Extrinsic Fabry–Perot Interferometer Pressure Sensor. IEEE Sens J 2016;16:3396. https://doi.org/10.1109/JSEN.2015.2434772

[30] Marques CAF, Peng GD, Webb DJ. Highly sensitive liquid level monitoring system utilizing polymer fiber Bragg gratings. Opt Express 2015;23:6058. https://doi.org/10.1364/OE.23.006058.

[31] Leal-Junior A, Theodosiou A, Frizera A, Pontes MJ, Shafir E, Palchik O, Tal N, Zilberman S, Berkovic G, Antunes P, Andre P, Kalli K, Marques C. Characterization of a new polymer optical fiber with enhanced sensing capabilities using a Bragg grating. Opt Lett 2018;43:4799. https://doi.org/10.1364/OL.43.004799.

[32] Cheng X, Liu Y, Yu CY. Gas pressure sensor based on BDK-doped polymer optical fiber. Micromachines 2019;10:717. https://doi.org/10.3390/mi10110717.

[33] De M, Gangopadhyay TK, Singh VK. Prospects of photonic crystal fiber as physical sensor: An overview. Sensors 2019;19. https://doi.org/10.3390/s19030464.

[34] Zheng Y, Shum PP, Liu S, Li B, Xiang Y, Luo Y, Zhang YN, Ni WJ, Wu ZF, Dinh XQ, Zeng, SW, Auguste J, Humbert G. Experimental and numerical investigation on hollow core photonic crystal fiber based bending sensor. Opt Express 2019;27:30629. https://doi.org/10.1364/oe.27.030629.

[35] Muller GM, Frank A, Yang L, Gu X, Bohnert K. Temperature Compensation of Interferometric and Polarimetric Fiber-Optic Current Sensors with Spun Highly Birefringent Fiber. J Light Technol 2019;37:4507. https://doi.org/10.1109/JLT.2019.2907803.

[36] Naeem K, Kim BH, Kim B, Chung Y. Simultaneous multi-parameter measurement using Sagnac loop hybrid interferometer based on a highly birefringent photonic crystal fiber with two asymmetric cores. Opt Express 2015;23:3589. https://doi.org/10.1364/oe.23.003589.

[37] Li X, Cao H, Chang Z, Zhang X, Zhao W, Shen R. A fiber optic ultrasonic sensor using polarization-maintaining fiber for partial discharge monitoring. Sens Mater 2019;31:1407. https://doi.org/10.18494/SAM.2019.2260.

[38] Primak W, Post D. Photoelastic constants of vitreous silica and its elastic coefficient of refractive index. J Appl Phys 1959;30:779–88. https://doi.org/10.1063/1.1735231.

[39] Shin-Etsu Quartz Products Co., Ltd. Quartz Glass for Optics. https://www.sqp.co.jp/e/catalog/images/QuartzGlass_for_Optics_e.pdf

[40] Huang JY, Van Roosbroeck J, Vlekken J, Martinez AB, Geernaert T, Berghmans F, Hoe BV, Lindner E, Caucheteur C. FBGs written in specialty fiber for high pressure/high temperature measurement. Opt Express 2017;25:17936. https://doi.org/10.1364/OE.25.017936、

[41] Sharma M, Dixit V, Konar S, Ahmed K and Dhasarathan V. Endlessly single-mode photonic crystal fiber with high birefringence for sensing applications. Mod Phys Lett B 2020;Online Ready. https://doi.org/10.1142/S0217984920500773